

Journal of Materials Chemistry B

Polycyclic aromatic polymer nanoparticles show potent infectious particle adsorption capability

Journal:	Journal of Materials Chemistry B			
Manuscript ID	TB-ART-08-2024-001793.R1			
Article Type:	Paper			
Date Submitted by the Author:	10-Oct-2024			
Complete List of Authors:	Oishi, Yudai; Kumamoto University, Faculty of Advanced Science and Technology Toyoda, Mako; Kumamoto University, Joint Research Center for Human Retrovirus Infection Hano, Nanami; Kumamoto University, Faculty of Advanced Science and Technology; IROAST Motozono, Chihiro; Kumamoto University, Joint Research Center for Human Retrovirus Infection Ueno, Takamasa; Kumamoto University, Joint Research Center for Human Retrovirus Infection Takafuji, Makoto; Kumamoto University, Faculty of Advanced Science and Technology; IROAST,			

SCHOLARONE™ Manuscripts

ARTICLE

Polycyclic aromatic polymer nanoparticles show potent infectious particle adsorption capability†

Received 00th January 20xx, Accepted 00th January 20xx

DOI: 10.1039/x0xx000000x

Yudai Oishi,^{a‡} Mako Toyoda,^{b‡} Nanami Hano,^{ac} Chihiro Motozono,^b Takamasa Ueno^b and Makoto Takafuji*^{ac}

Nonspecific viral adsorption by polymer nanoparticles is more economical and superior in terms of operating cost and energy efficiency than viral adsorption using virus-specific antibodies and filtration techniques involving size exclusion in the order of tens of nanometres. In this study, we synthesised four types of polycyclic aromatic polymer (ArP) nanoparticles with different structures and evaluated their virus adsorption capability for infectious particles of the newly emerged severe acute respiratory syndrome coronavirus 2 (SARS-CoV-2). ArP nanoparticles with a diameter of approximately 500 nm were prepared by one-pot precipitation polymerisation using structural isomers of bifunctional dihydroxynaphthalene (1,5-dihydroxynaphthalene and 2,6-dihydroxynaphthalene) as phenol monomers, as well as 3-hydroxybenzoic acid and 3-aminophenol as comonomers to introduce carboxylic acid and amino groups, respectively. This wide range of phenolic monomers offers a powerful molecular design capability, enabling the optimisation of surface properties for the adsorption of various infectious virus particles. The virus adsorption capacity of the ArP nanoparticles exceeded 20,000 plaque-forming units and was found to be correlated with the nitrogen (primary and secondary amines) and quinone contents on the ArP nanoparticle surface. Furthermore, a polyvinylidene difluoride membrane filter uniformly coated with the ArP nanoparticles could remove viruses by filtration in a flow system.

Introduction

Polymer nanoparticles have applications in various fields, including chemical synthesis, electronics, medicine, and agriculture. In the medical field, they are used for separation, adsorption, analysis, and immunoassays, and their particle size and interfacial functions are optimised for each application.^{1–3} Through surface modification with organic molecules and polymers, inorganic and metallic nanoparticles acquire high antimicrobial activity and adsorption capacity for bacteria, viruses, and others.^{4–6} Virus adsorption is especially important in processes requiring virus removal, such as the preparation of biopharmaceuticals, which should be free from viral contamination,⁷ and purification of drinking water from waterborne viruses such as hepatitis A virus, norovirus, rotavirus, and adenovirus.⁸ Various virus removal technologies with varying degrees of sophistication, operating cost, removal

efficiency, and energy consumption have been reported. These technologies mainly involve mechanical and electrical filtration using, for example, ceramic filters, 9-11 coagulation processes, 12 photocatalytic disinfection, 13,14 ozone generators and UV irradiation, 15 chemical disinfection, and membrane-based processes. 16 Adsorption-based technologies are the least expensive and most efficient. 17 However, for economic reasons, specific adsorbents with covalently or ionically bonded virus-specific antibodies are unsuitable for mass processing. Thus, nonspecific virus adsorbents with long-term durability and high thermal stability, which would allow recycling by heating, must be developed.

Polymer nanoparticles have advantages as nonspecific virus adsorbents, such as greater molecular designability, precise control of particle size and chemical structure, long-term dispersion stability, and higher biocompatibility. 18,19 Various polymer nanoparticles have been reported as viral adsorbents, such as the composite *N*-heterocyclic polymer and silver nanoparticles; 20 'confetti'-like nanoparticles synthesised by dispersion copolymerisation; 21 porous polymer particles functionalised with C–O, C=O, O–C=O, and –NH groups via plasma modification; 22 chitosan nanoparticles; 23 and polystyrene particles substituted with various amino acids. 24

According to the many experimental approaches presented above, physical adsorption based on the interaction between the solid surface and the spike (S) protein on the viral surface is promoted by not only enlarging the specific surface area of the solid, but also introducing ionic functional groups such as –COOH and –NH₂, as well as random conformations of

^{a.} Faculty of Advanced Science and Technology, Kumamoto University, 2-39-1 Kurokami, Chuo-ku, Kumamoto 860-8555, Japan. E-mail: takafuji@kumamotou ac in

b. Division of Infection and Immunity, Joint Research Center for Human Retrovirus Infection, Kumamoto University, 2-2-1, Honjo, Chuo-ku, Kumamoto 860-0811, Japan.

International Research Organization for Advanced Science and Technology (IROAST), Kumamoto University, 2-39-1 Kurokami, Chuo-ku, Kumamoto 860-8555, Japan.

[†] Electronic Supplementary Information (ESI) available: [Preparation conditions, XPS, Zeta–potential, FE-SEM, EDX and TGA for ArP nanoparticles]. See DOI: 10.1039/x0xx00000x

[‡] These authors contributed equally to this work.

these groups, to create active sites that specifically interact with the S protein. However, these experimental approaches have not been directly compared with each other due to the different targets and methods of the virus adsorption tests. Furthermore, because of the complexity and diversity of the interaction between viral and solid surfaces, a theoretical approach to the overall mechanism is also difficult.^{25,26} Therefore, there is an urgent need for novel virus adsorbents with high molecular designability to allow easy optimisation of their chemical structures for various targets.

We developed a new technique for the one-pot synthesis of polycyclic aromatic polymer (ArP) nanoparticles ranging from several tens of nanometres to several microns in size by heating and stirring phenolic compounds and heterocyclic amines in solution.^{27,28} The ArP nanoparticles have several characteristics: 1) surfactant-free synthesis, 2) spherical shape and high monodispersibility, 3) high dispersion stability in a wide range of solvents from water to nonpolar solvents, 4) high visibility due to deep colour, and 5) high thermal stability, which allows recycling by heating. Moreover, the ArP nanoparticles can form a coating layer on the solid surface of filter materials to endow them with virus adsorption capability.²⁹

The ArP nanoparticles we employed are synthesised through precipitation polymerisation of aromatic compounds and heterocyclic amines. It is possible to control the surface characteristics of nanoparticles by using various types of monomers because these monomers have multiple reactive sites (o-, p-, or m-position on aromatic compounds and N-position on heterocyclic amine) to introduce various functional groups. In contrast to previous methods, $^{20-24}$ this one-pot synthesis achieves high molecular designability, which should make it easy to improve the efficiency of virus adsorption on solid surfaces and optimise the nanoparticles for different viruses.

In this study, we tried to apply functionalised ArP nanoparticles as virus adsorbents. In a one-pot process, 1,5-(1,5-DHN) dihydroxy naphthalene 2,6dihydroxynaphthalene (2,6-DHN) was used as the monomer and 3-hydroxybenzoic acid (PhCOOH) or 3-aminophenol (PhNH₂) was used as the comonomer to introduce carboxylic acid and amino functional groups, respectively. Severe acute respiratory syndrome coronavirus 2 (SARS-CoV-2) was chosen as the viral target because its size (approximately 100 nm) makes it ideal for submicron-sized adsorption on the ArP nanoparticles. Additionally, we evaluated the SARS-CoV-2 filtering capacity of a polyvinylidene difluoride (PVDF) membrane filter modified with an ArP coating layer.

Experimental

Materials

1,5-DHN (>98.0%), 2,6-DHN (>95.0%), 1,3,5-trimethyl-1,3,5-triazinane (TMTA, >98.0%), PhCOOH (>98.0%), and PhNH $_2$ (>98.5%) were purchased from Tokyo Chemical Industry Co., Ltd. (Tokyo, Japan) and used without further purification.

Ethanol (EtOH, >99.0%), ethylene glycol (>99.5%), and 1butanol (>99.0%) were purchased from Fujifilm Wako Pure Chemical Corp. (Osaka, Japan) and used without further purification. 1-Propanol (>98.0%) was purchased from Nacalai Tesque, Inc. (Kyoto, Japan) and used as received. The clinically isolated SARS-CoV-2 Wuhan strain, SARS-CoV-2/Hu/DP/Kng/19-020 (GenBank accession no. LC528232) was provided by Drs Tomohiko Takasaki and Jun-ichi Sakuragi (Kanagawa Prefectural Institute of Public Health). The virus was propagated in VeroE6/TMPRSS2 cells (JCRB1819) in 10% foetal bovine serum (FBS)/low-glucose Dulbecco's modified Eagle's medium with L-glutamine and phenol red (Fujifilm Wako Pure Chemical Corp., Cat# 041-29775) containing 1 mg/mL G418 (Nacalai Tesque, Inc.) penicillin/streptomycin (Fujifilm Wako Pure Chemical Corp., Japan, Cat# 168-23191), and plaque-forming units (PFU) were determined by plaque assays. Real-time reverse transcription quantitative polymerase chain reaction (RT-qPCR) was performed using a One Step PrimeScript™ III RT-qPCR Mix (Takara Bio, Japan, Cat# RR600B) according to the manufacturer's instructions. Primer/Probe N2 (2019-nCoV) (Takara Bio, Japan, Cat# XD0008) was used as the primer and probe. The hydrophilic PVDF membrane filter Durapore®2 with a 0.45-µm pore size was purchased from Merck KGaA, Germany.

Preparation of functionalised ArP nanoparticles

In a general method, the monomers (1,5-DHN and 2,6-DHN) and comonomers (PhCOOH and PhNH₂) were dissolved in the desired solvent, placed in a 500-mL three-necked separable flask connected to a mechanical stirrer and reflux tube, and then heated at the reaction temperature. TMTA was dissolved in a small amount of the desired solvent and poured into the reactor. After heating and stirring for the appropriate reaction time, the resultant ArP nanoparticles were filtered through a 0.1-µm polytetrafluoroethylene membrane filter, washed several times with EtOH, and vacuum dried. All conditions (solvent, temperature, and reaction time) were optimised to control the particle size (450-600 nm) and are summarised in Table S1. The ArP nanoparticles synthesised from 1,5-DHN, 2,6-DHN, 1,5-DHN/PhCOOH, and 1,5-DHN/PhNH₂ were denoted as 15D, 26D, 15D-C, and 15D-N, respectively. Heat treatment of the ArP nanoparticles was carried out at 150 °C under N2 atmosphere for 2 h to remove small-molecularweight residuals. The corresponding ArP nanoparticles were denoted as 15D-h, 26D-h, 15D-C-h, and 15D-N-h.

Characterisation of ArP nanoparticles

The size and morphology of the ArP nanoparticles were examined by scanning electron microscopy (SEM; JCM-5700, JEOL, Japan). Elemental analysis (Micro Corder JM10, J-Science Lab Co., Ltd., Japan) was performed to identify the elements in the nanoparticles. Fourier-transform infrared (FT-IR) measurements were conducted using an FT-IR spectrometer (FT/IR-4100, Jasco, Japan) equipped with a diffuse reflectance accessory (DR PRO410-M, Jasco, Japan). The zeta potential of the ArP nanoparticles in the aqueous dispersion was measured

Journal Name ARTICLE

by electrophoretic light scattering (Zetasizer Nano ZS, Spectris, UK). The chemical bonding state of the ArP nanoparticles was investigated by high-resolution X-ray photoelectron spectroscopy (HR-XPS; K-Alpha, Thermo Fisher Scientific Inc., USA). The samples were pressed onto pure indium foil, and HR-XPS analyses were performed using a monochromatised Al K α X-ray source with an energy of 1486.6 eV. During the measurements, the vacuum pressure was 10^{-6} Pa and the pass energy for the high-resolution spectra was 40 eV. Energy-dispersive X-ray spectroscopy (EDX) analysis was performed using a Genesis APEX2 detector (Ametek Co., Ltd., USA) installed on a field emission scanning electron microscope (SU8000, Hitachi, Ltd., Japan).

Surface modification of membrane filters

Hydrophilic PVDF membrane filters were immersed in a 30 mM 1,5-DHN–TMTA–EtOH solution and shaken at 50 °C for up to 6 h in an incubator shaker. Samples were collected every hour, washed several times with EtOH, and dried under vacuum.

Characterisation of surface-modified membrane filters

The morphologies of the surface-modified membrane filters were examined using a JCM-5700 scanning electron microscope. The diffuse reflectance spectra of the membrane filters were measured using a UV-3600 Plus spectrophotometer equipped with an ISR-603 integrating sphere attachment (Shimadzu Co., Japan). The surface zeta potentials of the membrane filters were measured by electroosmotic flow mapping (Zetasizer Nano ZS with surface zeta potential cell kit ZEN1020, Spectris, UK) using a standard latex dispersant in pH 9.2 buffer as the tracer particles.

Evaluation of the cytotoxicity of ArP nanoparticles

The cytotoxicity of the ArP nanoparticles to Vero cells was evaluated using Cell Counting Kit-8 (CCK-8; Dojindo Laboratories, Japan). Briefly, 1×10^4 Vero cells (JCRB0111) in 10% FBS/Eagle's minimum essential medium with L-glutamine and phenol red (Fujifilm Wako Pure Chemical Corp., Cat# 051-07615) were seeded in a 96-well plate the day before the experiment, and then the supernatant of a polymer solution dissolved in water and sonicated was added to a final concentration of 1 mg/mL. After culturing for 72 h, the cells were incubated with 10 μ L of CCK-8 reagent for 3 h at 37 °C. The absorbance was measured at 450 nm using an iMark microplate absorbance reader (Bio-Rad, USA).

Adsorption of SARS-CoV-2 by ArP nanoparticles

Fig. 1 shows a schematic representation of the experimental procedure for virus adsorption. We performed a plaque assay to detect viral titres and RT-qPCR to detect and quantify viral RNA, as described previously. 30,31 For the plaque assay, 1×10^5 Vero cells were seeded in a 24-well plate the day before infection. The next day, 180 μL of a sonicated solution of ArP nanoparticles dispersed in water was mixed with 1,620 μL of a virus-containing serum-free dilution buffer composed of 20 mM 4-(2-hydroxyethyl)-1-piperazine ethanesulfonic acid

(Nacalai Tesque, Inc.), 1X minimum essential medium (Thermo Fisher Scientific, USA), 1X non-essential amino acids solution (Thermo Fisher Scientific), and 1% penicillin/streptomycin. The final concentration of ArP nanoparticles was 1.0 mg/mL, and the virus concentrations were 4,000, 20,000, and 40,000 PFU/mL. After 1-h incubation at 37 °C, the mixed solution was centrifuged at 14,000 rpm for 5 min, and the virus-containing supernatant was collected. The Vero cells were then exposed to 250 μL of the supernatant at 37 $^{\circ} C$ for 2 h. The cell monolayer was then overlaid with 1 mL of 1.5% carboxymethyl cellulose (Wako Pure Chemical Industries, Ltd., Japan) in a buffer supplemented with 3% FBS. After 3 days, the cells were fixed with 4% paraformaldehyde in phosphate buffered saline and stained with 0.25% crystal violet (Bio Medical Science Ltd., Japan). After the stained cells were washed with water and dried, the number of plaques was counted using an ImmunoSpot S6 analyser (M&S TechnoSystems, Japan). For RT-qPCR, 5 μ L of the virus-containing supernatant was mixed with 5 µL of a 2X RNA lysis buffer [2% Triton X-100 (Nacalai Tesque, Inc., Cat# 35501-02), 50 mM KCl, 100 mM Tris-HCl (pH 7.4), 40% glycerol, and 0.4 U/µL recombinant RNasin® RNase inhibitor (Promega Corp., Cat# N2615)] and incubated at 25 °C for 10 min. RNase-free water (90 μ L) was added, and the diluted sample (3 µL) was used as the template for RT-qPCR performed using a One Step PrimeScript™ III RT-qPCR Mix. The viral RNA copy number was standardised using a Positive Control RNA Mix (2019-nCoV) (Takara Bio, Cat# XA0142). Fluorescent signals were acquired using a LightCycler® 96 system (Roche Diagnostics GmbH, Germany).

The viral adsorption ratio was calculated using Eq. 1,

Viral adsorption ratio (%) =
$$(V_0 - V_s)/V_0 \times 100$$
, (1)

where V_0 is the initial viral RNA copy number or PFU and V_s is the viral RNA copy number or PFU in the supernatant after virus adsorption.

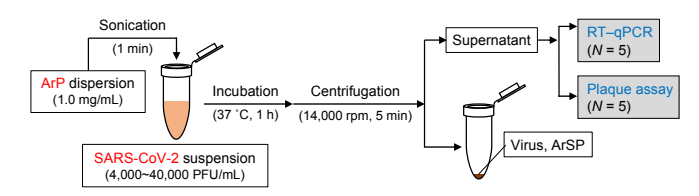


Fig. 1 Schematic representation of virus adsorption procedure.

Virus filtration by surface-modified membrane filters

To determine the viral adsorption ratios of the ArP-coated PVDF membrane filters [0 (untreated), 2, and 4 h immersion], the membrane filters were cut into 13-mm-diameter circles, mounted in syringe filter holders (SWINNEX® \mathbb{Z} , Merck KGaA, Germany), and placed on 5-mL syringes. For the virus filtration method, 2 mL of a SARS-CoV-2 suspension (4,000 PFU/mL) was injected into the syringe and filtered through the syringe filter, and the residual amount of virus in the filtrate was evaluated by plaque assays (N = 4) and RT-qPCR (N = 4). The flow rate was manually controlled to be as constant as possible.

Results and discussion

One-pot synthesis of ArP nanoparticles

Fig. 2 summarises the synthesis route of the ArP nanoparticles, namely 15D, 26D, 15D-C, and 15D-N. Their chemical structures were reported previously.²² In this study, the monomer was 1,5-DHN (15D), and PhCOOH or PhNH₂, which has carboxyl or amino groups, respectively, was added as the comonomer (15D-C and 15D-N, respectively) to enhance the electrostatic interactions between the nanoparticles and S proteins on the virus surface. 2,6-DHN was also used as a monomer (26D) to investigate a new interaction mode between the hydroxy groups on the nanoparticle surface and viruses. The comonomers and 2,6-DHN required longer reaction times because of their lower reactivity compared to 1,5-DHN. By optimising the solvent, reaction temperature, and reaction time, yields of more than 30% were obtained (Table S1). Additionally, the polymers were heat-treated (15D-h, 26D-h, 15D-C-h, and 15D-N-h) to remove unreacted monomers and low-molecular-weight oligomers, which would reduce cytotoxicity.

Fig. 2 Chemical structures of the monomers and synthesis routes of the ArP nanoparticles.

Characterisation of ArP nanoparticles

The particle sizes measured from the SEM images (Fig. 3) and elemental compositions of the ArP nanoparticles are summarised in Table 1. By optimising the reaction conditions, the average size of the nanoparticles was controlled to 450-600 nm. However, only 26D showed a wide size distribution. This is because 2,6-DHN had a much slower reaction rate than 1,5-DHN; therefore, nucleation and growth proceeded simultaneously (i.e., nucleation occurred continuously in the later stages of the reaction). Moreover, because of heat treatment, the particle size decreased slightly. Elemental analysis showed that the elemental composition ratios, particularly the C/N ratios, of the nanoparticles were considerably different. 15D-N, which was synthesised using PhNH₂ as the comonomer, had the highest nitrogen content, even after heat treatment (15D-N-h). Thus, a certain amount of PhNH₂ was likely incorporated into 15D-N. Furthermore, although 15D-C was synthesised using PhCOOH as the comonomer, which does not have a nitrogen atom, it had the second-highest nitrogen content. This could be due to the

unexpected incorporation of TMTA-derived nitrogen into 15D-C. $\label{eq:total_condition}$

 Table 1 Particle sizes and elemental compositions of ArP nanoparticles before and after heat treatment.

	Particle size		Elemental analysis			
Name	d	CV	H (%)	C (%)	N (%)	C/N
	(nm)	(%)	П (%)	C (%)	IN (%)	C/N
15D	448	7.9	5.76	65.8	6.69	9.8
15D-h	446	7.4	5.64	66.8	6.64	10.1
26D	481	31.8	5.20	69.9	5.27	13.3
26D-h	487	27.4	5.22	71.0	5.39	13.2
15D-C	617	4.6	6.02	67.1	7.89	8.5
15D-C-h	607	4.8	5.30	68.2	7.84	8.7
15D-N	667	5.0	5.70	62.6	10.31	6.1
15D-N-h	654	5.6	4.99	64.7	9.97	6.5

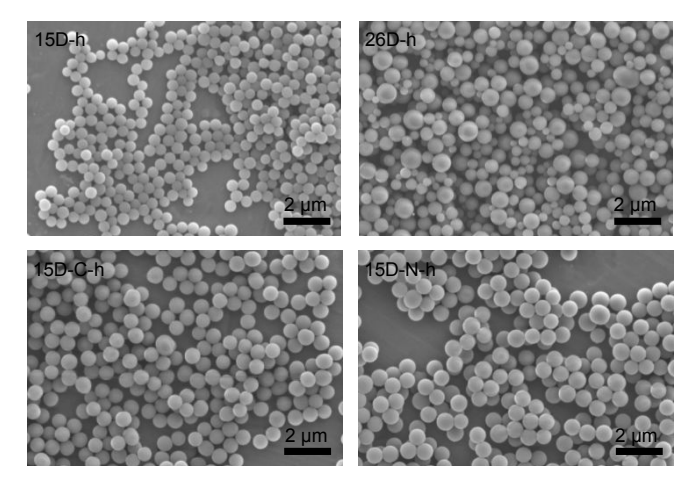


Fig. 3 SEM images of ArP nanoparticles after heat treatment.

Fig. 4 shows the FT-IR spectra of the ArP nanoparticles after heat treatment. All nanoparticles exhibited a broad peak at 3500–3700 cm⁻¹ attributed to the O–H stretching vibration of the hydroxyl groups of 1,5-DHN/2,6-DHN, and a peak at 2960 cm⁻¹, attributed to the C–H stretching vibration of the –CH₃ or –CH₂ groups of TMTA. For all particles, a peak at 1659 cm⁻¹ appeared at the same position as the C=O stretching peak of 1,4-naphthoquinone, indicating that some of the monomers were reduced to a quinone-type structure. 15D-C-h exhibited a weak peak at 1689 cm⁻¹, which was attributed to the C=O stretching vibration of the carboxyl group of PhCOOH. 15D-N-h exhibited a strong peak at 3340 cm⁻¹, which was attributed to the N–H stretching vibration of the amino group of PhNH₂.

XPS and EDX measurements were performed for all four particles. The XPS survey spectra of the ArP nanoparticles showed three peaks at 284.9–285.1, 399.9–400.1, and 532.0–532.8 eV, corresponding to C 1s, N 1s, and O 1s, respectively (Fig. S1). Thus, N atoms were observed in all particles, and their content increased in the order 26D-h < 15D-h < 15D-C-h < 15D-N-h (Table S2), similar to the elemental analysis results. The trend in N% observed from EDX analysis of the surface of the ArP nanoparticles (Fig. S2 and Table S3) was also consistent with these results. These findings suggest that N atoms were distributed on the surface of the particles at varying contents.

Journal Name ARTICLE

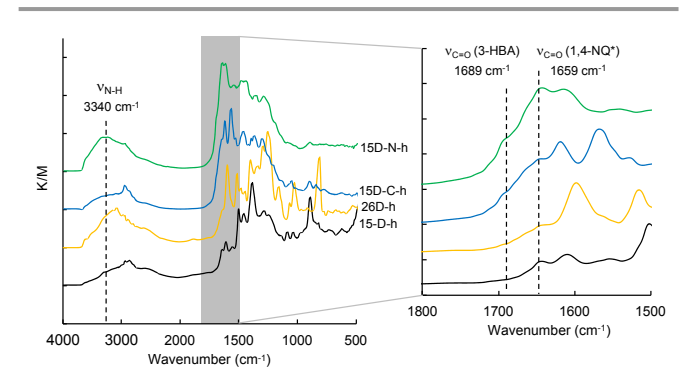


Fig. 4 FT-IR spectra of ArP nanoparticles after heat treatment.

The HR-XPS spectra showed a relatively higher content of secondary amines in 15D-C-h and 15D-N-h and primary amines in 15D-N-h, which may be relevant to virus adsorption (Fig. 5 and Table S4). In addition, the XPS spectra indicated the presence of C=O bonds in all the particles, suggesting that the O bonded to the benzene ring forms a quinone structure (Table S5). C=O bonds derived from carboxylic acids were expected to be detected in 15D-C-h; however, the highest C=O ratio was observed for 15D-N-h. These results suggest that hydrogen bonding between quinone moieties (C=O) and S proteins is effective for virus adsorption.

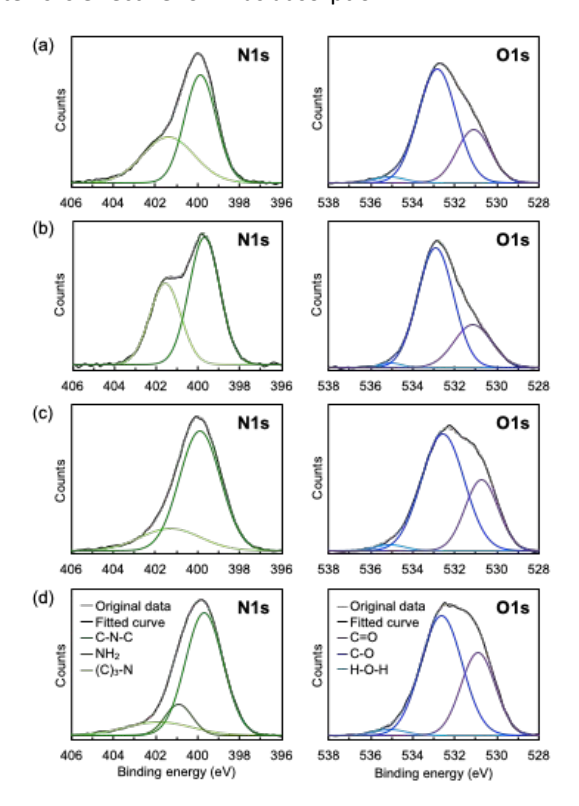


Fig. 5 High-resolution N 1s and O 1s XPS spectra of ArP nanoparticles. (a) 15D-h, (b) 26D-h, (c) 15D-C-h and (d) 15D-N-h.

Table S6 summarises the surface zeta potentials of the ArP nanoparticles. Most of the conditions (pH, ionic strength, particle concentration, and dispersion method) were the same as those of the virus adsorption experiment. All nanoparticles

had a negative charge of similar magnitude at pH 7.5. These results indicate that the carboxyl and amino groups introduced into 15D-C and 15D-N, respectively, did not significantly affect the surface charge at pH 7.5.

Cytotoxicity of ArP nanoparticles to Vero cells

Before conducting virus adsorption tests of the ArP nanoparticles, their potential cytotoxic effect on Vero cells was evaluated. Fig. 6 shows the viability of Vero cells (1 \times 10 4 cells) 72 h after exposure to 1 mg/mL of ArP nanoparticle dispersion. All samples, except that exposed to 15D, had comparable viability to the control without nanoparticle treatment. The viability of Vero cells exposed to the 15D dispersion after 72 h was 75.8%; however, it increased up to 100% after heat treatment (15D-h). Comparing the compositions of 15D and 15D-h obtained by thermogravimetric analysis (Fig. S3), the difference in weight loss at 150 °C was approximately 3%, suggesting that heat treatment of 15D removed unreacted monomers and other low-molecular-weight compounds. These results indicate that although the low-molecular-weight residue, such as amines derived from TMTA, captured in 15D exhibits severe cytotoxicity, it is efficiently removed by heat treatment. At 1 mg/mL, the heat-treated ArP nanoparticles had little effect on cell proliferation. Therefore, this concentration was chosen for subsequent virus adsorption tests.

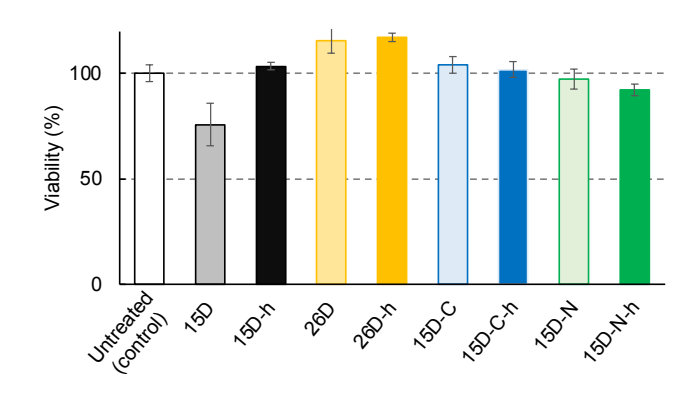


Fig. 6 Viability of Vero cells after exposure to 1 mg/mL of ArP nanoparticle aqueous dispersion for 72 h at 37 °C. All colour reaction values are normalized to that of the control (no ArP nanoparticle exposure), which represents 100% cell viability. The error bar represents standard deviation.

Adsorption of SARS-CoV-2 by the ArP nanoparticles

Fig. 7 shows the results of the plaque assays of the supernatants after virus adsorption by 1.0 mg/mL of different ArP nanoparticles (15D-h, 26D-h, 15D-C-h, and 15D-N-h) using SARS-CoV-2 aqueous suspensions with different viral titres (4,000, 20,000, and 40,000 PFU/mL). For initial viral titres of 20,000 and 40,000 PFU/mL, the supernatant was diluted to 1/5 and 1/10, respectively, for the plaque assay (4th and 5th rows in Fig. 7) because the number of "virus only" plaques was uncountable (2nd and 3rd rows in Fig. 7).

Fig. 8 shows the viral adsorption ratios calculated using the viral RNA copy number measured by RT-qPCR (N = 5) and viral titre determined by the plaque assay (N = 5) of the

supernatants. For initial viral titres of 4,000 and 20,000 PFU/mL, the viral adsorption ratios were 100% (plaque assay) and 99% (RT-qPCR), indicating that virus adsorption onto the nanoparticle surface was not saturated under those conditions. When the initial viral titre was 40,000 PFU/mL, virus residue was detected, and the viral adsorption ratio increased in the order 15D-h < 26D-h = 15D-C-h < 15D-N-h.

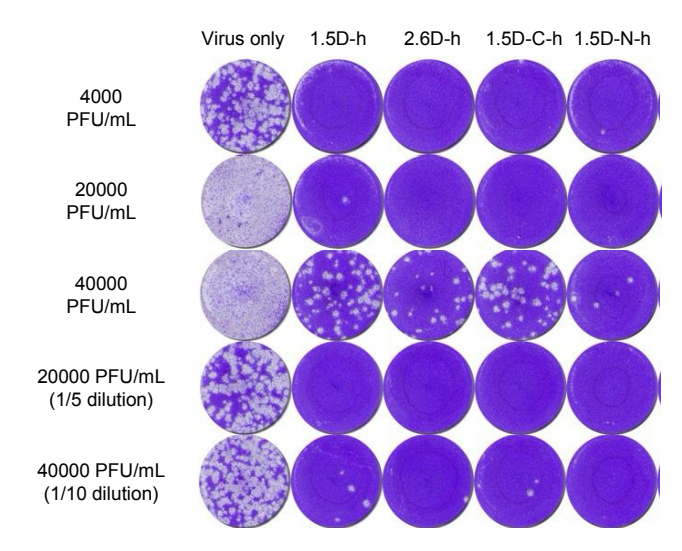


Fig. 7 Results of the plaque assays of supernatants after virus adsorption by ArP nanoparticles using SARS-CoV-2 aqueous suspensions with different initial viral titres.

Based on the particle diameters listed in Table 1, the specific surface area increased in the order 15D-N-h < 15D-C-h < 26D-h < 15D-C, which was the opposite order of the viral adsorption ratio. This indicates that the viral adsorption ratio depends more strongly on the chemical and steric structures of the nanoparticle surface than on the specific surface area of the nanoparticles. In contrast, the nitrogen content increased in the order 26D-h < 15D-h < 15D-C-h < 15D-N-h (Table 1), indicating that the viral adsorption ratio is strongly correlated with the nitrogen content. A plot of the virus adsorption ratio against the nitrogen content obtained from elemental analysis confirmed this correlation for the three ArP nanoparticles prepared using 1,5-DHN (Fig. S4). However, 26D-h had a high viral adsorption ratio despite its low nitrogen content because 1) it has a different hydroxyl group conformation from 1,5-DHN and 2) it has a relatively positive charge, which has a favourable effect on its interaction with the virus. The nitrogen atoms derived from TMTA are considered to form imine groups (CH₂-N(CH₃)-CH₂-), which can donate electrons to the naphthalene ring. However, the negative charge on the particle surface did not increase with the increase of these imine groups (Table S6). Furthermore, there are no previous reports of higher virus adsorption due to increased imine groups. Two reasons may explain why more imine groups enhanced viral adsorption here: 1) the relatively strong basicity of imine groups allows electrostatic interactions with the carboxyl groups in the S protein and 2) a higher crosslinking density enhances multiple interactions between functional groups on the particles (hydroxy, amino, and carboxyl groups) and the S protein.

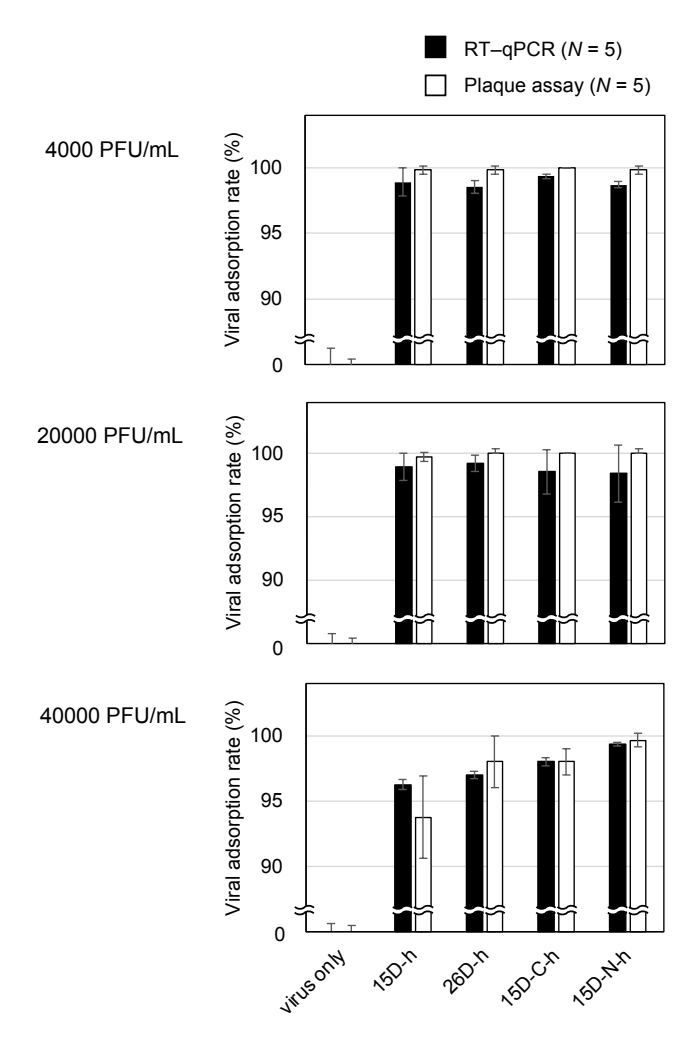


Fig. 8 Viral adsorption ratios calculated using the viral RNA copy number (RT-qPCR, N = 5) and viral titre (plaque assay, N = 5). The error bar represents standard deviation.

Surface modification of the PVDF membrane filter

Immersing a PVDF membrane filter in an EtOH solution of 1,5-DHN and TMTA turned the colour of the solution from colourless to light pink after approximately 1 h, transparent wine after approximately 3 h, and brown after approximately 4 h. Particles with diameters of approximately 800 nm were generated, as determined by dynamic light scattering. Colouration of the membrane filter was visually observed from 3 to 4 h, as shown in Fig. 9(a).

Characterisation of the surface-modified membrane filter

Fig. 9(b) shows SEM images of the hydrophilic PVDF membrane filter after surface modification. The PVDF membrane filter consisted of a network of fibrils (several hundred nanometres in diameter) with voids less than 1 μm , and this morphology did not change even after 6 h of reaction. Fig. 10(a) shows the reaction time dependence of the diffuse reflectance spectrum of the membrane filter. The intensity of

Journal Name ARTICLE

the absorption peak at 546 nm (Fig. 10(b)), attributed to the ArP coating, increased

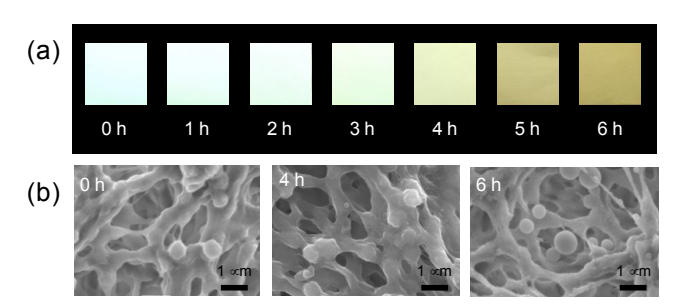


Fig. 9 (a) Photographs and (b) SEM images of PVDF membrane filter after surface modification with 1,5-DHN and TMTA.

significantly between 3 and 4 h. These results are consistent with the changes in colour (Fig. 9(a)). The surface zeta potential of the membrane filter in pH 9.2 buffer solution was -32.0 mV (R^2 = 0.955) before surface modification, -42.7 mV (R^2 = 0.949) after 2 h of immersion, and -79.0 mV (R^2 = 0.944) after 4 h of immersion. This significant increase in negative charge was attributed to the negative charge of the ArP coating layer (Table S6). These results indicate that the polymerisation of 1,5-DHN and TMTA in the presence of PVDF can quantitatively coat the PVDF surface with a thin-film thickness. This implies that the pore properties are maintained after polymer coating, which can be deployed in various substrates such as filters and porous materials.

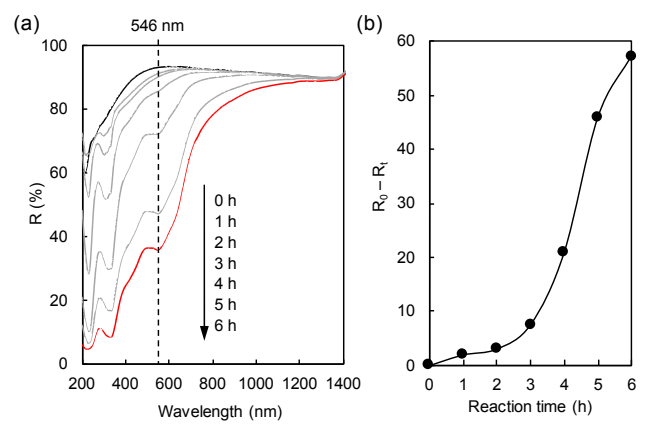


Fig. 10 (a) Diffuse reflectance spectrum of PVDF membrane filter after surface modification for 1–6 h. (b) Time-dependent difference spectrum (R_0 - R_1) at 546 nm, where R_0 and R_1 are the reflectance of the PVDF membrane filter immersed for 0 and t h, respectively.

Virus filtration by surface-modified PVDF membrane filters

Fig. 11 shows the viral adsorption ratios of the ArP-coated PVDF membrane filters. The viral adsorption ratio of the untreated hydrophilic PVDF membrane filter (PVDF-0h) was ~30% because the pore size was 0.45 μm , which is sufficiently larger than the virion size. In contrast, the viral adsorption ratio increased to ~50% after modification for 2 h (PVDF-2h) and to ~60% after modification for 4 h (PVDF-4h). This was attributed to the more negative surface zeta potential inside the membrane filter due to the ArP coating. Analysis of the

adsorption of the S protein on polystyrene by all-atom molecular dynamics simulations revealed that this process is mainly driven by hydrophobic and $\pi-\pi$ interactions with amino acid residues such as valine and phenylalanine. 26 ArPs contain atoms such as N and O, and their chemical structures are considered to be more complex. Nevertheless, it may be possible to analyse their interactions with the S protein using the above-mentioned analytical method in the future.

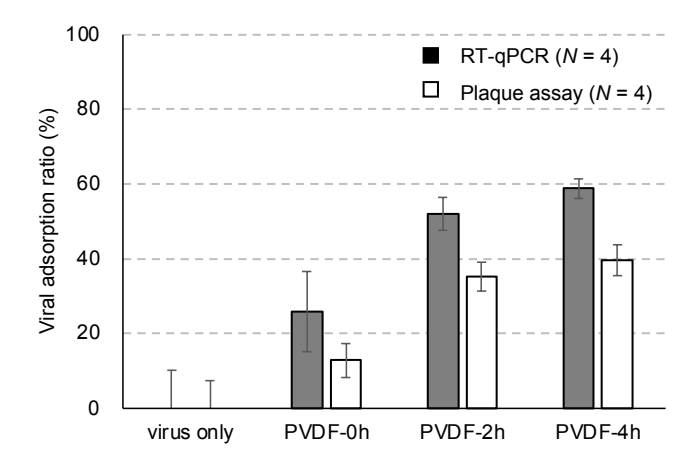


Fig. 11 Viral adsorption ratios of untreated and surface-modified PVDF membrane filters calculated using the viral RNA copy number (RT-qPCR, N = 4) and viral titre (plaque assay, N = 4). The error bar represents standard deviation.

Conclusions

In this study, ArP nanoparticles for SARS-CoV-2 adsorption were synthesised by one-pot precipitation polymerisation using various phenolic monomers. The four obtained particles were spherical with a diameter of approximately 500 \pm 100 nm. The viral adsorption ratio was more than 99%, even when 20,000 PFU of virus per 1 mg of nanoparticles was added. When 40,000 PFU of virus was added, the viral adsorption ratio increased in the order 15D-h < 26D-h = 15D-C-h < 15D-N-h. Zeta potential measurements at around pH 7.5 indicated that the surface charges of all polymer nanoparticles used in this study were negatively charged with similar magnitude (-36 to -31 mV), which prompted a more detailed characterisation of the particle surface structure. The results of elemental, XPS, and EDX analyses confirmed that the higher the ratio of primary amines, secondary amines, and quinones on the naphthalene ring on the particle surface, the greater the amount of virus adsorption. Moreover, the position of the hydroxyl group on the naphthalene ring contributed to virus adsorption. The synthesis method for ArPs can be applied to various phenols, including natural polyphenols, and functional groups can be easily introduced. By utilising a technique that can synthesise spherical nanoparticles with various functional groups and polymer backbones in one pot, the chemical and three-dimensional structures can be controlled according to the adsorption target. In addition, an ArP coating layer was introduced to a commercially available PVDF membrane filter by immersing the filter in a solution of 1,5-DHN and TMTA. As the immersion time increased, the surface zeta potential of

the membrane filter became negative, confirming that the polymer was coated onto the filter surface. The virus adsorption rate of the polymer-coated membrane filter increased to approximately 60%, compared to 30% for the uncoated membrane filter. This successful virus adsorption in a flow system indicates that the polymer coating can be applied to column and membrane separation systems, and further research and development is expected in the future.

Author Contributions

Yudai Oishi: Investigation, Validation, Formal analysis, Writing original draft, Visualisation; Mako Toyoda: Investigation, Validation, Formal analysis, Writing - original draft, Visualisation; Nanami Hano: Investigation, Validation, Formal analysis, Visualisation, Writing - Review & Editing; Chihiro Motozono: Methodology, Writing - Review & Editing, Resources; Takamasa Ueno: Methodology, Writing - review & editing, Supervision, Funding acquisition, Resources; Makoto Takafuji: Conceptualisation, Methodology, Writing - review & editing, Supervision, Resources, Project administration, Funding acquisition.

Conflicts of interest

There are no conflicts to declare.

Data Availability

The data supporting this article have been included as part of the Supplementary Information.

Acknowledgements

This study was supported by JST A-STEP, Japan (Grant Number JPMJTR21T3). We would like to thank Editage (www.editage.jp) for English language editing.

References

- 1 S. Andrade, M. J. Ramalho and J. A. Loureiro, *Polymers*, 2024, **16**, 249.
- Z. Song, Z. Han, S. LV, C. Chen, L. Chen, L. Yin and J. Cheng, Chem. Soc. Rev., 2017, 46, 6570–6599.
- N. Singh, S. Son, J. An, I. Kim, M. Choi, N. Kong, W. Tao and J. S. Kim, Chem. Soc. Rev., 2021, 50, 12883–12896.
- 4 T. D. Pham, P. T. Nguyen, T. M. N. Phan, T. D. Dinh, T. M. H. Tran, M. K. Nguyen, T. H. Hoang and A. L. Srivastav, *Environ. Res.*, 2024, 258, 119396.
- 5 T. Hou, S. S. Sana, D. V. Kumbhakar, H. Li, V. K. N. Boya, M. A. S. Aly, Z. Zhang and T. D. Pham, J. Drug Delivery Sci. Technol., 2023, 87, 104799.
- 6 T. T. T. Truong, T. T. M. Tran, T. K. C. Tran, T. N. Vu, T. D. Dinh, L. Tran, T. M. V. Nguyen, T. T. Truong, T. H. Y. Doan and T. D. Pham, J. Mol. Liq., 2023, 386, 122538.
- 7 S. T. Andreadis, C. M. Roth, J. M. Le Doux, J. R. Morgan and M. L. Yarmush, *Biotechnol. Prog.*, 1999, 15, 1–11.
- Z. Altintas, M. Gittens, J. Pocock and I. E. Tothill, *Biochimie*, 2015, **115**, 144–154.

- B. Michen, A. Diatta, J. Fritsch, C. Aneziris and T. Graule, *Sep. Purif. Technol.*, 2011, **81**, 77–87.
- B. Michen, J. Fritsch, C. Aneziris and T. Graule, *Environ. Sci. Technol.*, 2013, 47, 1526–1533.
- 11 K. P. Goswami and G. Pugazhenthi, J. Environ. Manage., 2020, 268, 110583.
- 12 N. Shirasaki, T. Matsushita, Y. Matsui, K. Murai and A. Aochi, *J. Hazard. Mater.*, 2017, **326**, 110–119.
- 13 C. Zhang, Y. Li, D. Shuai, Y. Shen and D. Wang, *Chem. Eng. J.*, 2019, **355**, 399–415.
- 14 A. Habibi-Yangjeh, S. Asadzadeh-Khaneghah, S. Feizpoor and A. Rouhi, *J. Colloid Interface Sci.*, 2020, **580**, 503–514.
- 15 E. Cheek, V. Guercio, C. Shrubsole and S. Dimitroulopoulou, *Sci. Total. Environ.*, 2021, **766**, 142585.
- 16 B. Wu, R. Wang and A. G. Fane, *Water Res.*, 2017, **110**, 120–132
- 17 L. Sellaoui, M. Badawi, A. Monari, T. Tatarchuk, S. Jemli, G. L. Dotto, A. Bonilla-Petriciolet and Z. Chen, *Chem. Eng. J.*, 2021, **412**, 128682.
- 18 I.-Y. Jeon and J.-B. Baek, Materials, 2010, 3, 3654-3674.
- 19 S. Martano, V. De Matteis, M. Cascione and R. Rinaldi, Nanomaterials. 2022, 12, 2337.
- 20 V. T. Ivanova, E. O. Garina, E. I. Burtseva, E. S. Kirillova, M. V. Ivanova, J. Stejskal and I. Yu. Sapurina, *Chem. Pap.*, 2017, 71, 495–503.
- 21 K. Hamada, T. Kaneko, M. Q. Chen and M. Akashi, *Chem. Mater.*, 2007, **19**, 1044–1052.
- 22 N. Aikeremu, S. Li, Q. Xu, H. Yuan, K. Lu, J. Si and D. Yang, Appl. Sci., 2022, 12, 12628.
- 23 J. Ciejka, K. Wolski, M. Nowakowska, K. Pyrc and K. Szczubiałkab, *Mater. Sci. Eng. C*, 2017, **76**, 735–742.
- 24 E. Imbert-Laurenceau, M.-C. Berger, G. Pavon-Djavid, A. Jouan and V. Migonney, *Polymer*, 2005, **46**, 1277–1285.
- 25 L. Xie, F. Liu, J. Liu and H. Zeng, ACS Appl. Mater. Interfaces, 2020, 12, 58360–58368.
- 26 M. Sahihi and J. Faraudo, *J. Chem. Inf. Model.*, 2022, **62**, 3814–3824.
- 27 A. Murakami, H. Noguchi, Y. Kuwahara, M. Takafuji, S. Nozato, R. Sun, A. Nakasuga and H. Ihara, Chem. Lett., 2017, 46, 680–682.
- 28 N. Hano, M. Takafuji, H. Noguchi and H. Ihara, *ACS Appl. Nano Mater.*, 2019, **2**, 3597–3605.
- 29 H. Noguchi, T. Liu, S. Nozato, Y. Kuwahara, M. Takafuji, S. Nagaoka and H. Ihara, *Chem. Lett.*, 2017, **46**, 1233–1236.
- 30 Y. Maeda, M. Toyoda, T. Kuwata, H. Terasawa, U. Tokugawa, K. Monde, T. Sawa, T. Ueno and S. Matsushita. *Int. J. Mol. Sci.*, 2024, **25**, 1353.
- 31 M. Toyoda, T. S. Tan, C. Motozono, G. Barabona, A. Yonekawa, N. Shimono, R. Minami, Y. Nagasaki, Y. Miyashita, H. Oshiumi, K. Nakamura, S. Matsushita, T. Kuwata and T. Ueno, *Microbiol. Spectrum*, 2023, **11**, e00660-23.

Data Availability Statement

Polycyclic aromatic polymer nanoparticles show potent infectious particle adsorption capability

Yudai Oishi, a‡ Mako Toyoda, b‡ Nanami Hano, ac Chihiro Motozono, b Takamasa Uenob and Makoto Takafuji*ac

- a. Faculty of Advanced Science and Technology, Kumamoto University, 2-39-1 Kurokami, Chuo-ku, Kumamoto 860-8555, Japan.
 E-mail: takafuji@kumamoto-u.ac.jp
- b. Division of Infection and Immunity, Joint Research Center for Human Retrovirus Infection, Kumamoto University, 2-2-1, Honjo, Chuo-ku, Kumamoto 860-0811, Japan.
- c. International Research Organization for Advanced Science and Technology (IROAST), Kumamoto University, 2-39-1 Kurokami, Chuo-ku, Kumamoto 860-8555, Japan.

Raw data were generated at Kumamoto University, Japan. Derived data supporting the findings of this study are available from the corresponding author [M. T.] on request.